Extremely High Saturation Current-Bandwidth Product Performance of a Near-Ballistic Uni-Traveling-Carrier Photodiode With a Flip-Chip Bonding Structure

Jin-Wei Shi, *Member, IEEE*, F.-M. Kuo, C.-J. Wu, C. L. Chang, Cheng-Yi Liu, Cheng Yu Chen, and Jen-Inn Chyi, *Senior Member, IEEE*

***Abstract*—In this study, we demonstrate near-ballistic uni-traveling carrier photodiodes (NBUTC-PDs) with an optimized flip-chip bonding structure, wide 3-dB optical-to-electrical (O-E) bandwidth (>110 GHz), and extremely high saturation current-bandwidth product performance (37 mA, >110 GHz, >4070 mA·GHz). NBUTC-PDs with different active areas (28–144 μm^2) are fabricated and flip-chip bonded with coplanar waveguides onto an AlN-based pedestal. The overshoot drift velocity of the electrons in the collector layer of the NBUTC-PD means that both the thicknesses of the collector layer and active areas of our device can be increased to reduce the density of the output photocurrent, compared to that of the traditional UTC-PD. This improves the high power performance without seriously sacrificing the speed performance. According to the measured O-E frequency responses, devices with even a large active area (144 μm^2) can still have a flat O-E frequency response, from near dc to 110 GHz. A three-port equivalent circuit model for accurately extracting the 3-dB bandwidth of the devices is established. The extracted 3-dB O-E bandwidth of a device with a small active area (28 μm^2) can be as high as 280 GHz under a load of 25 Ω. In addition, the saturation current measurement results indicate that after inserting a center bonding pad on the pedestal (located below the p-metal of the NBUTC-PD for good heat sinking), the saturation current performance of the device becomes much higher than that of the control device (without the center bonding pad), especially for the device with a small active area (28 μm^2). The measurement and modeling results indicate that a device with a 144 μm^2 active area and optimized flip-chip bonding pedestal can achieve an extremely high saturation current-bandwidth product (6660 mA-GHz, 37 mA, 180 GHz).**

***Index Terms*—Flip-chip bonding, high-power photodiode (PD), photodiode.**

Manuscript received March 30, 2009; revised June 01, 2009 and June 25, 2009. Current version published December 04, 2009.

J.-W. Shi, F.-M. Kuo, C.-J. Wu, C.-Y. Chen, and J.-I. Chyi are with the Department of Electrical Engineering, National Central University, Jhongli 320, Taiwan (e-mail: jwshi@ee.ncu.edu.tw; 975201125@cc.ncu.edu.tw; 965201070@cc.ncu.edu.tw; 92501085@cc.ncu.edu.tw; chyi@ee.ncu.edu.tw).

C. L. Chang and C.-Y. Liu are with the Department of Chemical Engineering and Materials Engineering, National Central University, Jhongli 320, Taiwan (e-mail: 943204039@cc.ncu.edu.tw; chengyi@cc.ncu.edu.tw).

Color versions of one or more of the figures in this paper are available online at http://ieeexplore.ieee.org.

Digital Object Identifier 10.1109/JQE.2009.2027339

I. Introduction

HIGH-SPEED and high-power photodiodes (PDs) serve as key components in photonic millimeter-wave (MMW) communication systems [1] for transducing intense optical power to high-power MMW power. The saturation current-bandwidth product is thus a key parameter for evaluating the performance of the high-power PDs to be used for such applications, especially when the operating frequency is around 100 GHz or higher. In this high-frequency regime, a high-performance and low-cost MMW power amplifier, which can further increase the total output power from the photonic emitter as well as the transmission distance [1], [2], still remains a challenge. However, by increasing the saturation current of the PD, we can boost the injected optical power and further increase the maximum available MMW power. The burden imposed on the MMW power amplifier can be thus relaxed [2]. The key point to obtained the ultimate high saturation current-bandwidth product of the PD is to downscale the area of the photo-absorption active area and the thickness of the depletion layer. A thinner depletion layer leads to a shorter carrier transit time and a higher saturation current performance [2], [3]. However, the junction capacitance will also be increased, making downscaling of the device active area necessary to sustain low junction capacitance and achieve very high speed performance. However, device heating [4] and high parasitic resistance could become problems, seriously limiting the saturation current of a PD with such a small active area ($\sim 10\ \mu$m^2). It has been demonstrated that such problems can be minimized either by the incorporation of flip-chip bonding structures or an epitaxial layer transferring process [5]. With the exception of decreasing the thickness of the depletion layer, the only other way to shorten the carrier drift time is to let only electrons, which have much higher drift velocities than holes, be the active carriers in the epilayer structure of the PD. The uni-traveling carrier PD (UTC-PD) [1], [2], [6] has already demonstrated excellent saturation current-bandwidth product performance. UTC-PDs, with active areas downscaled to 13 μm^2, have demonstrated a 170-GHz optical-to-electrical (O-E) 3-dB bandwidth with a maximum output photocurrent of around 14 mA (2380 mA·GHz) [6], [7]. However, for such high output photocurrents, a high reverse-bias voltage (around

0018-9197/$26.00 © 2009 IEEE

-2 V) on the UTC-PD might be necessary, which would result in saturation of the electron drift velocity, and limit the saturation current-bandwidth product performance of the device. Near-ballistic UTC-PD (NBUTC-PD) structures have been demonstrated, which overcome this problem and further increase the drift velocity of the electrons [8], [9]. The insertion of an additional p-type charge layer into the collector layer of the UTC-PD means that the electrons can reach overshoot drift velocities even under high reverse-bias voltages and high output photocurrents [8]–[10]. In previous work [9], we have already disclosed on-wafer measurement results showing the excellent saturation-bandwidth product performance (2952 mA·GHz) of NBUTC-PDs at the W-band. In this study, we use an improved fabrication process, including flip-chip bonding techniques for packaging, and a modified epilayer structure for the NBUTC-PD. We further demonstrate great improvements in the speed and saturation current-bandwidth product performance of the device. An extremely high bandwidth (180 GHz) and a record high saturation current-bandwidth product performance (37 mA, >110 GHz, >4070 mA·GHz) were obtained for the flip-chip bonded NBUTC-PDs, better than those reported for UTC-PDs [6], [7], [11] (less than 3000 mA·GHz). These state-of-the-art results for the new NBUTC-PD flip-chip bonding structure can be attributed to increase the active area (144 μm^2 versus 13 μm^2) of the device, thereby minimizing the current density and reducing the parasitic resistance, leading to the significant phenomenon of ac capacitance reduction [10].

II. Device Structure and Measurement Setup

Fig. 1(a)–(d) shows the top view of the NBUTC-PD before flip-chip bonding, cross-sectional views of the demonstrated device, the flip-chip bonded NBUTC-PD, and the layout of the flip-chip bonding pedestal, respectively. The details of the geometric structure of the backside of the illuminated NBUTC-PD are similar to those described in our previous work [9]. The epistructure was grown by molecular beam epitaxy (MBE) on a semi-insulating (SI) InP substrate.[1] As shown in Fig. 1(b), the thickness of the p-type linear-graded doped (1×10^{19} (top) $\sim$ 2.5×10^{17} (bottom) cm^{-3}) $In_{0.53}Ga_{0.47}As$-based photo-absorption layer (P) is 150 nm. The large slope of the graded doping profile, which induces the appropriate built-in electric field (2.1–84 kV/cm), ensures the occurrence of electron drift for overshoot velocities ranging from a low output current density until saturation of the PD occurs [12]. A p-type $In_{0.52}Al_{0.29}Ga_{0.19}As$ diffusion blocking layer (2×10^{18} cm^{-3}) was inserted between the P-layer and the p^{+}-type ($> 5 \times 10^{19}$ cm^{-3}) InGaAs-based ohmic contact layer. A p^{+} $In_xGa_{1-x}As$ contact layer, with a graded indium mole fraction ($x = 0.53$ to $x = 0.8$), was adopted to further reduce the contact resistance. A 280-nm-thick n-type InP layer (2×10^{16} cm^{-3}) was utilized as the collector layer (C). A 90-nm-thick p-type doped (1.7×10^{17} cm^{-3}) $In_{0.52}Al_{0.48}As$-based layer served as the electric field buffer layer (charge layer) (E). It works on similar principles to the charge layer of an avalanche photodiode (APD) [13], controlling the maximum electric field in the InP collector layer, to produce the appropriate value needed to sustain the overshoot velocity of photogenerated electrons under various bias voltages and output photocurrents. According to our measurements and simulation results, the charge layer became fully depleted when the reverse bias exceeded the absolute value of -2 V [8]. The undoped graded bandgap layers ($In_xAl_yGa_{0.48-y}As$) at the P-C and C-E junctions were 20 nm thick, making a total thickness of the effective collector layer of 410 nm. A greater collector layer thickness should allow us to achieve a similar *RC*-limited bandwidth with a larger device active area, giving the benefit of better injected light coupling, improved alignment tolerance, and lower output photocurrent density. The flip-chip bonding pedestal was composed of an AlN substrate, with a high thermal conductivity and low dielectric loss. The three metal stripes served as the coplanar waveguides (CPWs). In the center of CPW lines, we inserted a bonding pad, 10 μm in diameter, as shown in Fig. 1(d), which was directly bonded to the p-metal of the PD for good heat sinking. The major challenge in this process was to avoid melting centralized bonding pad, which could diffuse outside the bonding region, and shorten the signal and ground lines of the CPW pedestal. Such problems were minimized by optimizing the composition of the flip-chip bonding pads, time and temperature of the flip-chip bonding process, and the geometric structure of our layout. A control device, which was flip-chip bonded with an AlN pedestal without the center bonding pad, was also fabricated for comparison. Note the two integrated CPW pads, as shown in Fig. 1(c), one for extracting the photogenerated RF signal from the PD and the other for integrating a wafer probe connected to a W-band 50 Ω termination (Agilent 85059-60019) and a bias tee (Anritsu SC7204). The effective load resistance of our device during measurement was equal to 25 Ω. Furthermore, as shown in Fig. 1(c), a substrate microlens, 300 μm in diameter, was fabricated using backside photolithography and a one-step wet chemical etching process [14] to increase the alignment tolerance and responsivity of flip-chip bonding PDs. Fig. 2 shows the responsivity measured at an optical wavelength of 1.55 μm, normalized by the maximum responsivity of each device measured at its center, as a function of distance from the center. The closed and open symbols represent devices with and without a substrate lens, respectively. As can be seen, we achieve a more than three times improvement in both alignment tolerance (6.5 μm versus 2 μm, 95% degradation) and responsivity (0.15 A/W versus 0.04 A/W), with a device with an active radius of 4 μm and a substrate microlens, compared with the same device without a microlens.

III. Measurement Results

Devices A, B, C, and D (with active areas of 28, 64, 100, and 144 μm^2, respectively) were fabricated, and then, flip-chip bonded onto the same AlN-based pedestal prior to investigating their dynamic and high power performance in detail. The measured dc responsivity of these four devices was the same, around 0.15 A/W at a 1.55 μm optical wavelength. The O-E frequency responses and photogenerated RF power of the devices were measured with a two-laser heterodyne beating system with three different MMW power sensor heads for a range from dc to 50 GHz, V-band (50–75 GHz) and W-band

[1]Intelligent Epitaxy Technology, Inc., TX.

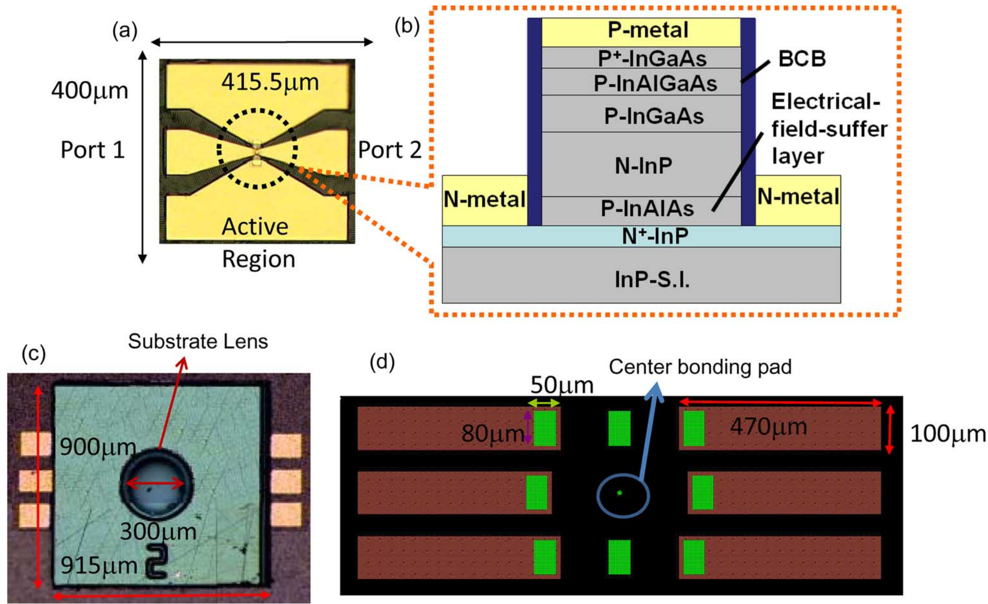

Fig. 1. (a) Top view of the NBUTC-PD. (b) Conceptual cross-sectional view of the NBUTC-PD. (c) NBUTC-PD after flip-chip bonding. (d) Flip-chip bonding pedestal.

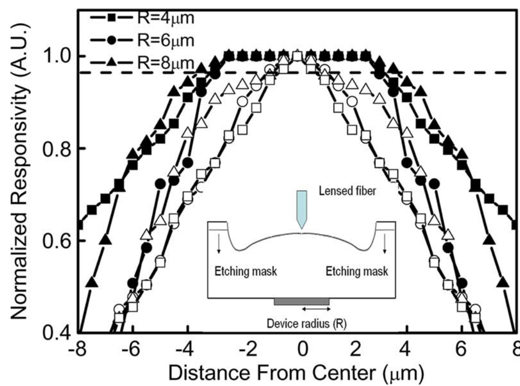

Fig. 2. Normalized responsivity versus the aligned position from the center of devices with different radii. The traces as indicated by open and closed symbols represent the devices without and with a substrate microlens, respectively.

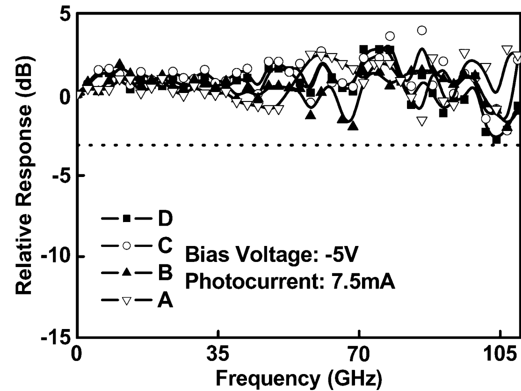

Fig. 3. Measured O-E frequency responses of devices A, B, C, and D under the same reverse-bias voltage (−5 V) and the same output photocurrent (7.5 mA).

(75–110 GHz). Traces A–D in Fig. 2 represent the measured O-E frequency responses of devices A–D. The output photocurrents (around 7.5 mA) and reverse-bias voltage (−5 V) are the same. As can be seen, all four devices (A, B, C, and D) exhibit flat O-E responses, from dc to near 110 GHz. In order to extract the 3-dB bandwidths of all these devices, we established a three-port equivalent circuit model [9], as shown in Fig. 4, to fit and extrapolate the measured O-E frequency responses. Region 1 and region 2 represent the bandwidth limitations of the carrier transit time (f_t) and the *RC* delay time (f_{RC}), respectively [9], [10]. Port 1 and port 2 in region 2 correspond to the two CPW flip-chip bonding pads shown in Fig. 1(c). The artificial *RC* network $[R_t, C_t, I(f)]$ in port 3 of region 1 represents the carrier transit time effect; the S_{31} or S_{32} parameter is equivalent to the net O-E frequency response. Our NBUTC-PD demonstrates an extracted carrier transit-time-limited bandwidth of over 400 GHz. The values and physical meaning of each component used in the fitting process of all four devices (A, B, C, and D) are shown in Table I. The parameters for the "pad simulation" blocks, indicated in this model, were calculated using momentum software. They are close in fit to the measured *S* parameters of a pair of dummy CPW pads on an AlN substrate. The established equivalent circuit model can be used to find the simulated frequency responses of the S_{11} and S_{21} parameters for our four devices (A, B, C, and D). The simulation results, all fit the measurement results very well. Fig. 5(a) and (b) shows the measured and fitted (simulated) frequency responses of the microwave (two electrical ports) S_{21} and S_{11} parameters of devices A and D, under a −3 V bias (see the Smith chart). Clearly, the simulated and measured results match very well, from near dc to 110 GHz, and the values of extracted parasitic resistance (R_p and R_n) are much smaller than those reported in our previous work [9]. Although there is some uncertainty in the extracted fitting values shown in Table I, we can clearly see that the measured S_{21} frequency response of both devices (as

TABLE I
LIST OF VALUES OF ELEMENTS USED IN THE FITTING PROCESS IN OUR EQUIVALENT CIRCUIT MODEL

	Physical Meaning	**Fitted Value**			
Size	**Active Area (μm²)**	**28**	**64**	**100**	**144**
Cco	**Capacitance of Collector Layer (fF)**	**7.1**	**15**	**23.44**	**34**
Csuff	**Capacitance of Electrical Field Suffer Layer (fF)**	**23.6**	**50**	**78**	**112.5**
L	**Parasitic Inductance (pH)**	**0.15**			
Cdx	**Parasitic Capacitance (fF)**	**0.14**			
Rco	**Resistance of Collector Layer (kΩ)**	**7.2**			
Rp	**P-type Contact Resistance (Ω)**	**1.2**			
Rn	**N-type Contact Resistance (Ω)**	**0.8**			
Pad Simulation	**The simulated S-parameters by using Momentum software**				

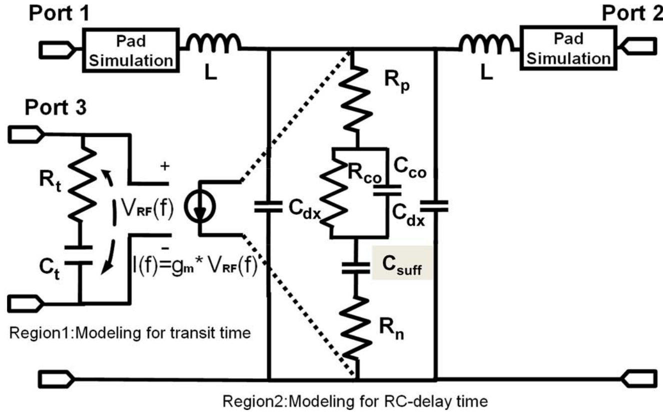

Fig. 4. Three-port equivalent circuit model of the NBUTC-PD.

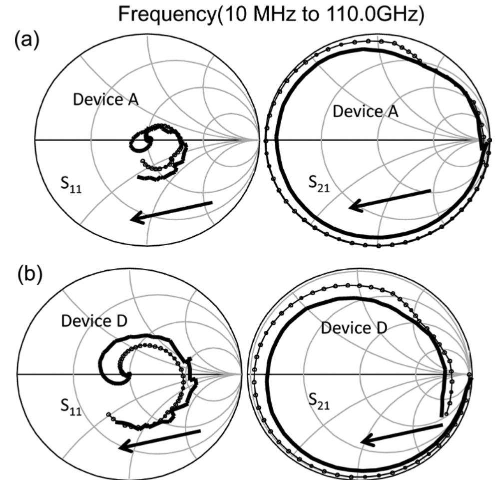

Fig. 5. Measured (continuous line) and fitted (open circles) S_{11} and S_{21} parameters for: (a) device A and (b) device D under a fixed dc bias voltage (-3 V) from near dc to 110 GHz. The arrowheads indicate an increase of the sweeping frequency.

shown on the Smith chart) is closer to the trace of ideal capacitance than the measured S_{21} traces reported in our previous work [9]. This result definitely indicates that our new device has a much smaller parasitic resistance than that of the device described in our previous work [9]. This improvement can be attributed to the reduction in contact resistance brought about by the introduction of the topmost p^+ $In_xGa_{1-x}As$ contact layer with graded indium mole fraction ($x = 0.53$ to $x = 0.8$). Further improvement in the etch-back process means that this new device also exhibits a much smaller parasitic capacitance (C_{dx}, 11 fF versus 0.14 fF) than that reported in our previous work [9]. Based on the established equivalent circuit model, we estimate the frequency response of our devices to be over 200 GHz. Fig. 6(a) and (b) shows the measured and fitted frequency responses for devices A, B and C, D, respectively. The ripples in the measured O-E frequency responses of both devices can be attributed to the multiple reflections between the flip-chip bonding pads and the active devices. The fitting of the measured S_{11}, S_{21}, and O-E frequency responses of devices without flip-chip bonding show that these ripples disappear when the frequency is below 300 GHz. The estimated bandwidths for devices A, B, C, and D are around 290, 280, 200, and 180 GHz, respectively. All the bandwidths are much larger than those of the previous device [9] (280 GHz versus 120 GHz). This device had the same active area (64 μm^2), so the improvement was due to the great reduction of parasitic capacitance and resistance, as discussed before. As compared to the reported UTC-PDs [6], [7] (under the same 25 Ω load), our NBUTC-PD achieves a larger 3-dB O-E bandwidth (280 GHz versus 170 GHz) with a much larger active area (64 μm^2 versus 13 μm^2). Our NBUTC-PD also has a smaller parasitic resistance, a more significant ac capacitance reduction [10], and a thicker collector layer to sustain the comparable value of junction capacitance. Fig. 7(a)–(d) shows the photogenerated RF power of devices A, B, C, and D, respectively, measured under a -3 V bias voltage. When the reverse-bias voltage is increased to -5 V, the photogenerated RF power from each device may increase further; however, the maximum saturation

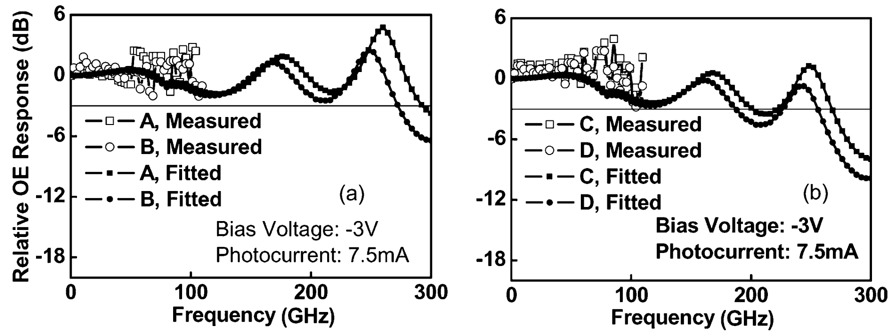

Fig. 6. Measured and simulated (fitted) frequency responses of: (a) devices A, B and (b) devices C, D under the same reverse-bias voltage (−3 V) and output photocurrent (7.5 mA).

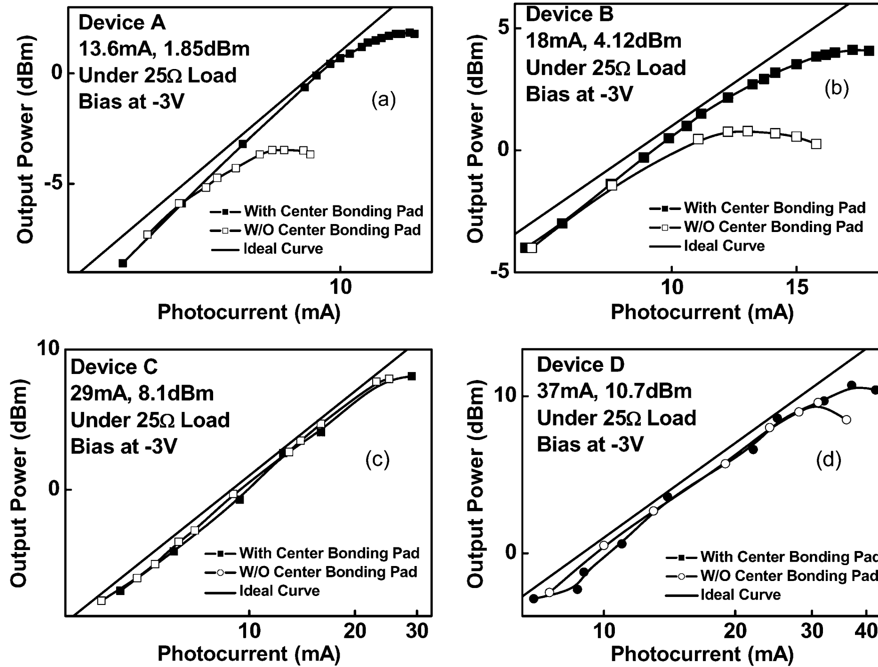

Fig. 7. Photogenerated RF power of devices: (a) A, (b) B, (c) C, and (d) D with and without center bonding pads versus photocurrent under a fixed reverse-bias voltage (−3 V) at 110 GHz.

current may not be improved, due to the increase of dissipated electrical power, which accompanies the thermal failure of the devices. The closed and open squares represent traces for flip-chip bonded devices with and without center bonding pads, respectively. The operating frequency was the same, 110 GHz, and limited by our W-band power sensor. The ideal relation between the RF power of a 100% modulated large signal and the average current for a 25 Ω equivalent load is also plotted (straight line) for reference. As can be seen, the insertion of an additional bonding pad in the center of the CPW lines of the device (for heat sinking), led to a higher saturation current than that of control device (without the center bonding pad). This phenomenon became more apparent when the active area of the device decreased. As can be seen in Fig. 7(a), under a −3 V bias voltage, the saturation current was around two times higher for the device with the smallest active area ($\sim 28\ \mu\text{m}^2$) and center bonding pads (13.6 mA versus 7.4 mA) than that of the control device. On the other hand, for device D, with a relative large ($144\ \mu\text{m}^2$) active area, the difference in saturation current (with and without the center bonding pad) was less apparent, only around 16% (31 mA versus 37 mA). The measured saturation density and saturation current-bandwidth produced under room temperature continuous-wave (CW) operation by devices A, B, C, and D are shown in detail in Table II. As can be seen, the maximum saturation density increases with the decrease of device active area. Based on these results, we can conclude that the significant difference in the measured saturation current between a small device (device A) with and without flip-chip bonding pads can be attributed to the increased output photocurrent density and thermal resistance of the devices, and the more serious problem of device heating when the active area of the device is downscaled. In addition, the measured saturation current-bandwidth product improves with increased device active area, which is contrary to the behavior reported for high-power UTC-PDs [11]. These high-power UTC-PDs usually have a thin collector layer (~230 nm) [11], accompanied by a large junction capacitance, which increases the maximum saturation output photocurrent. By further downscaling the device active area of traditional high-power UTC-PD, the *RC*-limited bandwidth can be greatly relaxed and a higher saturation current-

TABLE II
MEASURED BANDWIDTHS, BANDWIDTH-SATURATION CURRENT PRODUCTS, AND SATURATION CURRENT DENSITY FOR DEVICES A, B, C, AND D

Device	Bandwidth (GHz)	Saturation current(mA)	Bandwidth-Saturation current product (mA-GHz)	Saturation current density (kA/cm^2)
A	290	13.6	3944	45
B	280	18	5040	28
C	200	29	5800	29
D	180	37	6660	25.7

bandwidth product can be thus expected [11]. On the other hand, our NBUTC-PD has a relative thick collector layer (∼400 nm) and a more significant ac capacitance reduction phenomenon, which means that by enlarging the active area of the NBUTC-PD, we obtain a significant improvement in the output saturation current without serious degradation in the 3-dB bandwidth compared with that reported for high-power UTC-PDs [11]. The measured saturation-current bandwidth product of device D is record high, over 4070 mA·GHz (>110 GHz, 37 mA). This is superior to all values reported for high-performance evanescently coupled p-i-n PDs (624 mA·GHz, 120 GHz, 5.2 mA) [15], parallel-fed traveling wave photodetectors (1760 mA·GHz, 80 GHz, 22 mA) [16], and UTC-PDs [170 GHz [7] (50 GHz [11]), >14 mA [7] (50 mA [11]), >2380 mA·GHz [7], (2500 mA·GHz [11])] under the similar heterodyne-beating CW measurement. Extrapolating the bandwidth of our device, as shown in Fig. 2, the estimated saturation-bandwidth product should be around 6660 mA·GHz.

IV. Conclusion

In conclusion, we have demonstrated an NBUTC-PD, with flip-chip bonding on an AlN substrate for good heat sinking. Due to the higher electron drift velocity of our structure, we can increase the collector layer thickness and active area of the PD, which minimizes the current density and improves its high power performance. By introducing a center bonding pad in the flip-chip bonding pedestal for heat sinking, device D, with a 144 μm^2 active area, achieves a record high saturation current-bandwidth product [>110 GHz (180 GHz), 37 mA, >4070 mA·GHz (6660 mA·GHz)] for InP-based high-speed PDs.

References

[1] A. Hirata, T. Kosugi, H. Takahashi, R. Yamaguchi, F. Nakajima, T. Furuta, H. Ito, H. Sugahara, Y. Sato, and T. Nagatsuma, "120-GHz-band millimeter-wave photonic wireless link for 10-Gb/s data transmission," *IEEE Trans. Microw. Theory Tech.*, vol. 54, no. 5, pp. 1937–1944, May 2006.

[2] K. Kato, "Ultrawide-band/high-frequency photodetectors," *IEEE Trans. Microw. Theory Tech.*, vol. 47, no. 7, pp. 1265–1281, Jul. 1999.

[3] J.-W. Shi, H.-C. Hsu, F.-H. Huang, W.-S. Liu, J.-I. Chyi, J.-Y. Lu, C.-K. Sun, and C.-L. Pan, "Separated-transport-recombination p-i-n photodiode for high-speed and high-power performance," *IEEE Photon. Technol. Lett.*, vol. 17, no. 8, pp. 1722–1724, Aug. 2005.

[4] T. H. Stievater and K. J. Williams, "Thermally induced nonlinearities in high-speed p-i-n photodetectors," *IEEE Photon. Technol. Lett*, vol. 16, no. 1, pp. 239–241, Jan. 2004.

[5] N. Li, H. Chen, N. Duan, M. Liu, S. Demiguel, R. Sidhu, A. L. Holmes Jr., and J. C. Campbell, "High power photodiode wafer bonded to Si using Au with improved responsivity and output power," *IEEE Photon. Technol. Lett*, vol. 18, no. 23, pp. 2526–2528, Dec. 2006.

[6] H. Ito, S. Kodama, Y. Muramoto, T. Furuta, T. Nagatsuma, and T. Ishibashi, "High-speed and high-output InP-InGaAs uni-traveling-carrier photodiodes," *IEEE J. Sel. Topics Quantum Electron.*, vol. 10, no. 4, pp. 709–727, Jul./Aug. 2004.

[7] H. Ito, T. Furuta, F. Nakajima, K. Yoshino, and T. Ishibashi, "Photonic generation of continuous THz wave using uni-traveling-carrier photodiode," *J. Lightw. Technol.*, vol. 23, pp. 4016–4021, Dec. 2005.

[8] J.-W. Shi, C.-Y. Wu, Y.-S. Wu, P.-H. Chiu, and C.-C. Hong, "High-speed, high-responsivity, and high-power performance of near-ballistic uni-traveling-carrier photodiode at 1.55 μm wavelength," *IEEE Photon. Technol. Lett.*, vol. 17, no. 9, pp. 1929–1931, Sept. 2005.

[9] Y.-S. Wu and J.-W. Shi, "Dynamic analysis of high-power and high-speed near-ballistic uni-traveling carrier photodiodes at W-band," *IEEE Photon. Technol. Lett.*, vol. 20, no. 13, pp. 1160–1162, Jul. 2008.

[10] Y.-S. Wu, J.-W. Shi, and P.-H. Chiu, "Analytical modeling of a high-performance near-ballistic uni-traveling-carrier photodiode at a 1.55 μm wavelength," *IEEE Photon. Technol. Lett.*, vol. 18, no. 8, pp. 938–940, Apr. 2006.

[11] N. Li, X. Li, S. Demiguel, X. Zheng, J. C. Campbell, D. A. Tulchinsky, K. J. Williams, T. D. Isshiki, G. S. Kinsey, and R. Sudharsansan, "High-saturation-current charge-compensated InGaAs-InP uni-traveling-carrier photodiode," *IEEE Photon. Technol. Lett.*, vol. 16, no. 3, pp. 864–866, Mar. 2004.

[12] Y.-S. Wu, J.-W. Shi, P.-H. Chiu, and W. Lin, "High-performance dual-step evanescently-coupled uni-traveling-carrier photodiodes," *IEEE Photon. Technol. Lett.*, vol. 19, no. 20, pp. 1682–1684, Oct. 2007.

[13] J. C. Campbell, S. Demiguel, F. Ma, A. Beck, X. Guo, S. Wang, X. Zheng, X. Li, J. D. Beck, M. A. Kinch, A. Huntington, L. A. Coldren, J. Decobert, and N. Tscherptner, "Recent advances in avalanche photodiodes," *IEEE J. Sel. Topics Quantum Electron.*, vol. 10, no. 4, pp. 777–787, Jul./Aug. 2004.

[14] S. R. Cho, J. Kim, K. S. Oh, S. K. Yang, J. M. Baek, D. H. Jang, T. I. Kim, and H. Jeon, "Enhanced optical coupling performance in an InGaAs photodidoe integarted with wet-etched microlens," *IEEE Photon. Technol. Lett.*, vol. 14, no. 3, pp. 378–380, Mar. 2002.

[15] A. Beling, H.-G. Bach, G. G. Mekonnen, R. Kunkel, and D. Schmidt, "Miniaturized waveguide-integrated p-i-n photodetector with 120-GHz bandwidth and high responsivity," *IEEE Photon. Technol. Lett.*, vol. 17, no. 10, pp. 2152–2154, Oct. 2005.

[16] A. Beling, J. C. Campbell, H.-G. Bach, G. G. Mekonnen, and D. Schmidt, "Parallel-fed traveling wave photodetector for >100-GHz applications," *J. Lightw. Technol.*, vol. 26, pp. 16–20, Jan. 2008.

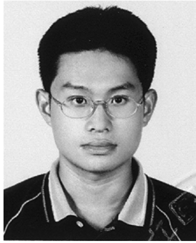

Jin-Wei Shi (M'02) was born in Kaohsiung, Taiwan, on January 22, 1976. He received the B.S. degree in electrical engineering from the National Taiwan University, Taipei, Taiwan, in 1998, and the Ph.D. degree from the Graduate Institute of Electro-Optical Engineering, National Taiwan University, in 2002.

From 2000 to 2001, he was a Visiting Scholar at the University of California, Santa Barbara. From 2002 to 2003, he served as a Postdoctoral Researcher at the Electronic Research and Service Organization (ERSO), Industrial Technology Research Institute (ITRI). In 2003, he joined the Department of Electrical Engineering, National Central University, Jhongli, Taiwan, where he is currently an Associate Professor. His research interests include ultrahigh speed/power optoelectronic devices, such as photodetectors, electro-absorption modulator, submillimeter-wave photonic transmitter, and semiconductor laser. He has authored or coauthored more than 60 journal papers and 100 conference papers. He holds 13 patents.

Dr. Shi was an invited speaker of the 2002 IEEE Lasers and Electro-Optics Society, the 2005 International Society for Optical Engineering Optics East, the 2007 Asia-Pacific Microwave Photonics Conference (AP-MWP), and the 2008 Asia Optical Fiber Communication and Optoelectronic Exposition and Conference. He was a member of the technical program committee of the Optical Fiber Communication Conference 2009 and 2010. He was the recipient of 2007 Excellence Young Researcher Award from the Association of Chinese IEEE.

F.-M. Kuo was born in Kaohsiung, Taiwan, on February 12, 1986. He received the B.S. degree in electrical engineering from the National Central University, Jhongli, Taiwan, where he is currently working toward the M.S. degree in electrical engineering. His research interests include millimeter-wave high-power photodiodes and semiconductor lasers.

C.-J. Wu was born in Kaohsiung, Taiwan, on August 3, 1984. She received the B.S. degree from the Department of Physics, National Kaohsiung Normal University, Kaohsiung, Taiwan. She is currently working toward the M.S. degree in electrical engineering at the National Central University, Jhongli, Taiwan. Her research interests include high-power photodiodes and flip-chip bonding process.

C. L. Chang is currently working toward the Ph.D. degree in the Department of Chemical and Materials Engineering, National Central University, Jhongli, Taiwan.

His research interests include LED chip fabrication and wafer bonding technology.

Cheng-Yi Liu received the Ph.D. degree in materials science and engineering from the University of California, Los Angeles.

He is currently a Full Professor in the Department of Chemical and Materials Engineering, National Central University, Jhongli, Taiwan. His research interests include IC packaging, and LED chip fabrication and packaging.

Cheng Yu Chen received the B.S. degree in 2007 from the Department of Electrical Engineering, National Central University, Jhongli, Taiwan, where he is currently working toward the Ph.D. degree.

His current research interests include II–VI materials epitaxy by molecular beam epitaxial system applied to optical devices.

Jen-Inn Chyi (M'94–SM'98) received the B.S. and M.S. degrees in electrical engineering from the National Tsing-Hua University, Hsin-Chu, Taiwan, in 1982 and 1984, respectively, and the Ph.D. degree in electrical engineering from the University of Illinois, Urbana-Champaign, in 1990.

In 1991, he joined the Department of Electrical Engineering, National Central University, Jhongli, Taiwan, where he was the Director of the Optical Sciences Center from 2000 to 2007; established molecular beam epitaxial (MBE), metal–organic vapor phase epitaxy (MOVPE), and high-speed optoelectronic devices laboratories, with house growth and characterization facilities for various III–V materials and devices; and is currently the Dean of the College of Electrical Engineering and Computer Science, and a Chair Professor of electrical engineering. His research interests include the areas of MBE and MOVPE growth of III–V semiconductors, and their heterostructures for high-speed electronic and optoelectronic devices. He has authored and coauthored more than 250 journal papers. He is the holder of 14 patents. His current research projects include MBE growth of InP-based heterojunction bipolar transisters, quantum-dot photonic devices, MOVPE growth of GaN-based materials for ultraviolet, blue, green emitters, and high-temperature, high-power devices.

Prof. Chyi is a member of the Phi Tau Phi. He is an Associate Editor of the IEEE PHOTONICS TECHNOLOGY LETTERS as well as the *Japanese Journal of Applied Physics.* He was a recipient of the 1996 Distinguished Young Researcher Award of the Electronic Devices and Materials Association of China, the 2002 Distinguished Research Award of the National Science Council of China, and the Distinguished Professor Award of the Chinese Institute of Electrical Engineering in 2004. He has been a Distinguished Lecturer of the IEEE Electron Devices Society since 2004.